Earthquakes and Structures, *Vol. 8, No. 3 (2015) 573-589*
DOI: http://dx.doi.org/10.12989/eas.2015.8.3.573

Scenario-based seismic performance assessment of regular and irregular highway bridges under near-fault ground motions

Abouzar Dolati[1a], Touraj Taghikhany[*1],
Mohammad Khanmohammadi[2b] and Alireza Rahai[1c]

[1]*Department of Civil and Environmental Engineering, Amirkabir University of Technology, Tehran, Iran*
[2]*School of Civil Engineering, College of Engineering, University of Tehran, Iran*

(Received November 1, 2013, Revised May 19, 2014, Accepted June 19, 2014)

Abstract. In order to investigate the seismic behavior of highway bridges under near-fault earthquakes, a parametric study was conducted for different regular and irregular bridges. To this end, an existing regular viaduct Highway Bridge was used as a reference model and five irregular samples were generated by varying span length and pier height. The seismic response of the six highway bridges was evaluated by three dimensional non-linear response history analysis using an ensemble of far-fault and scenario-based near-fault records. In this regard, drift ratio, input and dissipated energy as well as damage index of bridges were compared under far- and near-fault motions. The results indicate that the drift ratio under near-fault motions, on the average, is 100% and 30% more than far-fault motions at DBE and MCE levels, respectively. The energy and damage index results demonstrate a dissipation of lower energy in piers and a significant increase of collapse risk, especially for irregular highway bridges, under near-fault ground motions.

Keywords: highway bridge; pulse-like ground motion; 3-D non-linear modeling; irregular bridge

1. Introduction

Extensive damage of the engineering designed structures at the vicinity of seismic sources was the main purpose of many researches to understand the nature of ground motion in the surrounding areas of causative fault (Alavi and Krawinkler 2001). Their results have indicated that ground motions in the areas close to a ruptured fault can be significantly different from those further away from the seismic source. Similar researches demonstrated the role of pulse-like ground motions on seismic damage to high amplitude infrastructures such as highway bridges. Mays and Shaw (1997) studied seismic performance of 16-pier type bridges which were designed based on Seismic Design Criteria (SDC) 2006 (Caltrans 2006) under near-fault ground motions. The results of investigations conducted by Liao *et al*. (2000) illustrated that higher values of ductility and deformation demands are induced where near-fault pulse-like ground motions excite a five span

∗Corresponding author, Assistant Professor, E-mail: ttaghikhany@aut.ac.ir
[a]M.S. Student
[b]Assistant Professor
[c]Professor and Chair

http://www.techno-press.org/?journal=eas&subpage=7 ISSN: 2092-7614 (Print), 2092-7622 (Online)

sample bridge in comparison with far-fault earthquakes. In 2002, Orozco and Ashford conducted an experimental program on three bridge piers and investigated seismic behavior of the tested piers. They found that the plastic hinge length of piers in pulse-like earthquakes are smaller than those in far-fault non-pulse ones, but the ultimate strength and ductility are similar. Park *et al*. (2004) studied the Bolu Viaduct using crossing bridge scenario. They concluded that the near fault directivity pulses increases the seismic demand in energy dissipating units (EDU). Bonvalot (2006) in evaluation of the seismic performance of three different regular case study bridges concluded that the response of bridges is highly dependent upon the period content of this velocity pulse. He described, significant seismic damage may occur if the structure response is in tune with components of the forward directivity ground motion. Phan *et al*. (2007) conducted an experimental dynamic test on bridge piers and their results indicated large residual deformation under near-fault ground motions. Their test results demonstrated the residual deformation of pier under one directional near-fault pulse-like ground motions is more than that under ordinary earthquake which has low and bi-directional pulses. Kalkan and Kunnath (2006) compared the hysteretic energies of structures under near-fault and far-fault ground motions. Their study revealed higher deformation demand with low hysteretic energy of structural elements under near-fault ground motions.

Although understanding all effective parameters on seismic response of irregular bridges, particularly under pulse-like earthquake, demands a comprehensive investigation, the current research aims to maintain a general prospect regarding seismic performance of Highway Bridges. To this end, a case study box-girder highway bridge is carried out using a refined three dimensional model. Furthermore, to evaluate the effect of irregularity, five extra bridges have been designed by varying the dimensions of the case study in order to adopt irregularity of span ratio and pier's height in compliance with AASHTO (2007) provision. 3-D models of bridges assist to capture four different scenarios of near-fault ground motions in comparison with far-fault ones at DBE and MCE levels. The scenarios have been chosen based on fault rupture direction in relation to bridge position in order to study forward directivity pulses in each direction of piers. The seismic demand parameters such as drift ratio, hysteretic energy related to corresponding input energy and damage index (DI) of piers in different scenarios are computed in the longitudinal and transverse directions.

2. Description of analytical regular and irregular bridges

In order to provide a comprehensive study, a case study bridge has been selected as a reference model. The bridge is a segmental precast post-tensioned viaduct and is located in Tehran-Roodehen highway (Iran). The total length of the bridge deck is 215 meters and has been designed to be continuous through the three spans of 60, 95 and 60 meters. Fig. 1 shows the general view, cross section dimensions, and rebar arrangements of the reference bridge. Moreover, other important geometric parameters such as reinforcement ratios and axial load indices are listed in Table 1. The comparison between plastic shear and shear capacity reveals that the pier behavior in both longitudinal and transverse directions is controlled by flexure. Consequently, the effects of shear behavior on non-linear deformations were neglected and only flexural deformation was taken into consideration in modeling of piers.

In order to contribute to the irregular bridge behavior body of knowledge and generalize the results, the case study bridge is developed and five regular and irregular models are designed. The

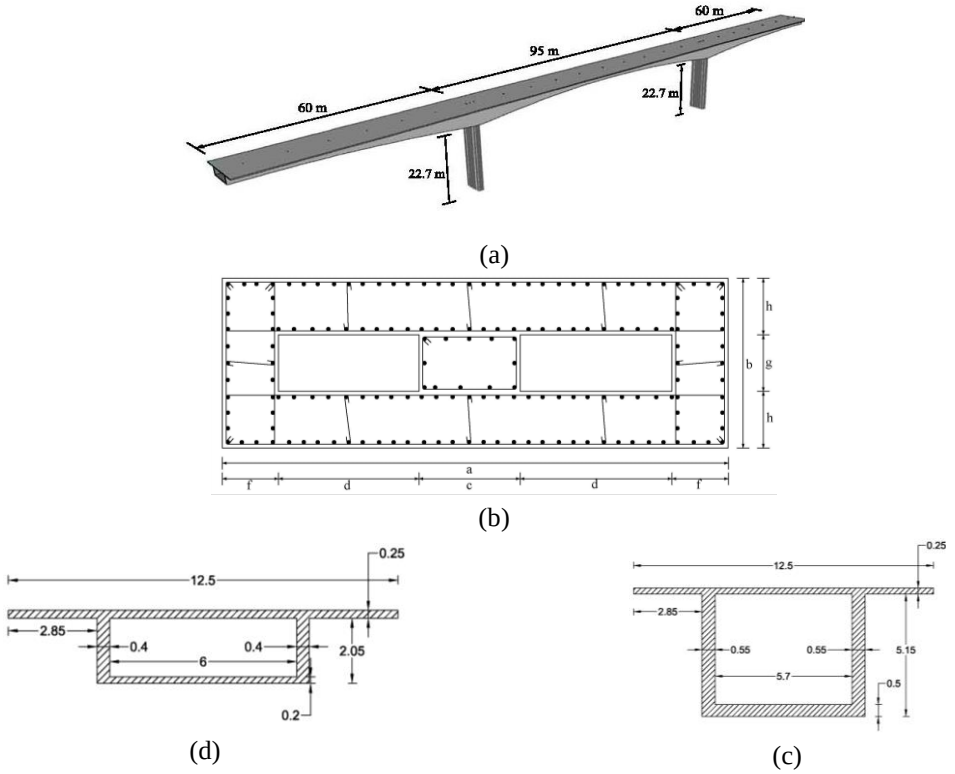

Fig. 1 Three-span case study regular bridge (a) general view, (b) piers cross section, (c) deck sections at top of the piers and (d) deck section at span

Table 1 Case study bridge properties

	Section dimension							ρ_L	ρ_T	AI	$V_{P\text{-}L}$	$V_{n\text{-}L}$	$V_{P\text{-}T}$	$V_{n\text{-}T}$
	a	b	C	D	f	g	H							
	m	m	M	M	m	m	M	%	%	%	kN.	kN.	kN.	kN.
Top	4.5	1.5	0.9	1.3	0.5	0.5	0.5	1.2	0.7	10.9	3166	12483	4609	11826
Bot	4.5	1.5	0.9	1.3	0.5	0.5	0.5	1.7	0.7	12.8				

ρ_L : Longitudinal reinforcement ratio
ρ_T : Transvers reinforcement ratio
AI : Axial indices($= P/f_c' A_g$)
$V_{P\text{-}L}$, $V_{P\text{-}T}$: plastic shear (associated with flexural plastic hinge) in longitudinal and transverse directions, respectively
$V_{n\text{-}L}$, $V_{n\text{-}T}$: Shear capacity according to SDC 2006 (Caltrans 2006) in longitudinal and transverse directions, respectively

new bridges were achieved by altering dimensions in the case study bridge, so that all possible irregularities in span and height according to AASHTO provisions could be achieved (see Fig. 2). Table 2 demonstrates all the relative stiffness values of piers in generated models. Models 2 and 5 represent span ratio irregularity and models 3 and 6 represent stiffness irregularity in the piers. All models were designed using AASHTO 2007 provisions and in order to have comparable results, axial load and DCR ratios are kept the same for all piers. Axial load indices (*AI*) are calculated using $AI=P/f'_c A_g$, where P is axial load due to the dead load plus half of the live load, f'_c is

Table 2 Relative stiffness ratios of piers, DCR ratios, and dynamic specification of designed bridges

Models No.	Longitudinal Direction			Transverse Direction			First Longitudinal Mode		First Transverse Mode	
	Pier No. 1	Pier No. 2	Pier No. 3	Pier No. 1	Pier No. 2	Pier No. 3	Period (Sec)	MPR*	Period (Sec)	MPR*
1	1.00	----	1.00	1.00	----	1.00	1.129	0.99	1.692	0.88
2	1.00	----	1.01	1.00	----	1.01	1.080	0.99	1.591	0.89
3	1.00	----	5.33	1.00	----	4.22	1.115	0.99	1.688	0.86
4	1.00	1.00	1.00	1.02	1.00	1.02	1.308	0.99	1.886	0.87
5	1.00	2.48	2.49	1.00	4.38	4.42	1.186	0.99	1.752	0.88
6	1.00	4.65	22.19	1.00	3.79	14.17	1.265	0.97	1.902	0.81

*MPR: Mass Participation Ratio

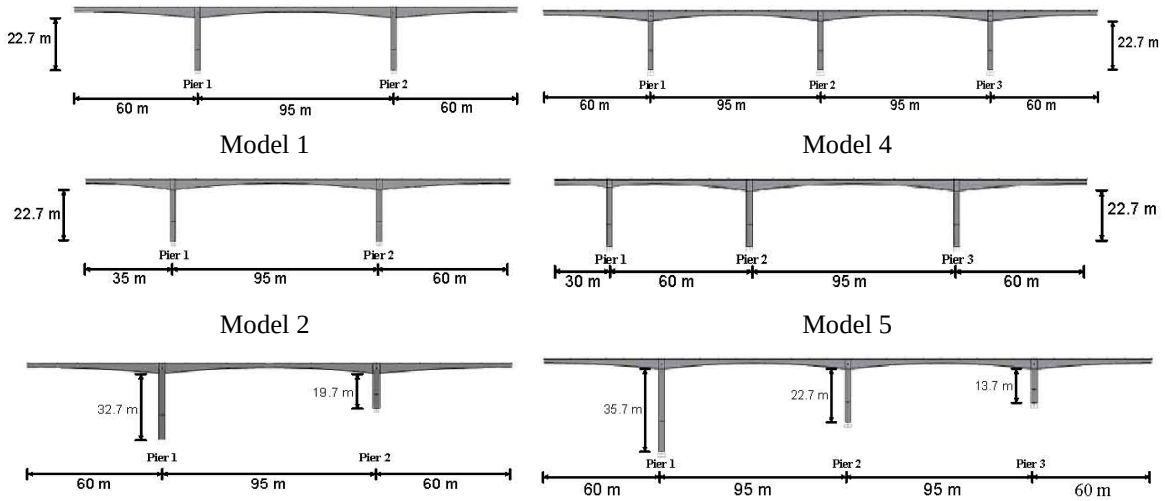

Fig. 2 Three- and four-span designed bridge models

compression strength and A_g is cross section area of the pier. Moreover, the percentage of longitudinal reinforcement was changed in all designed models in order to justify DCR ratio, while dimensions of piers were kept the same as the regular bridge.

3. Modeling of the bridges

To investigate the seismic behavior of described highway bridges, a set of 3-D non-linear models were developed using OpenSees code (Mckenna *et al*. 2010). In order to model the post-tensioned deck girders, an "elastic beam-column" element with equivalent specifications of non-cracked prismatic elements in accordance with SDC 2006 (Caltrans 2006) was used. The mass of deck has been lumped over adequate selected nodes along the deck. Due to the minor importance of the post tensioning effect in the response of the bridge, it was neglected in the modeling. Piers

have been modeled by using "beam with Hinges" elements to provide their non-linear behavior with plastic hinge length according to SDC 2006 (Caltrans 2006) for rectangular sections. In order to consider bi-directional interaction behavior of pies, the fiber section has been employed in plastic hinge regions. Concrete behavior in fiber model has been divided into confined and un-confined parts generated using Mander *et al*. (1998) model. Furthermore, "steel02" has been used to construct a uniaxial Giuffre-Menegotto-Pinto steel material object with isotropic strain hardening for rebar model. In order to consider limit state in material behavior, the generated stress-strain response has been limited. Regarding expected confinement of pier's sections, the concrete fibers' strain limit state at core and cover have been considered 0.013 and 0.006, respectively. Moreover, the strain limit states of about 2% in compression and 6% in tension have been considered for rebar material. Based on the sensitivity analysis to achieve suitable accuracy in moment curvature behavior, the fibers are assumed equal to 15×15 cm. Viscous Rayleigh damping with a damping ratio of 2% has been considered for analysis (Sadrossadat-Zadeh and Saiidi 2007). In order to consider the second order analysis effects, P-Delta option has been included in non-linear dynamic analysis of bridges. Furthermore, the structure interaction at foundation level has been neglected in compliance with SDC 2006 (Caltrans 2006) recommendations for ordinary bridges.

Interaction between deck and abutment is considered by using a suitable model which has been illustrated in Fig. 3. The abutment contains a rigid element supported by three springs in each direction at both ends. The longitudinal springs consider the response of gap (5 cm) and the embankment fill, where passive pressures are produced by the abutment back wall. "Hyperbolic Gap Material" has been assigned for elastic-perfectly-plastic (EPP) backbone curve of longitudinal response reported by SDC 2006 (Wilson and Elgamal 2006). In the presented model, the effects of backfill and wing wall on transverse direction have been taken into consideration using factors corresponding to wall effectiveness (*CL*) of 2/3 and participation coefficients (*Cw*) of 4/3 (Maroney and Chai 1994). The transverse ultimate strength is limited to 30% of vertical dead load applied at abutment according to SDC 2006. Moreover, Elastic No Tension spring (ENT) has been assigned at each end of the rigid link in order to present the vertical response. The compression stiffness has been assumed to be equal to the bearing pad stiffness. Furthermore, a rigid soil condition is also considered for beneath the abutments (Aviram *et al*. 2008).

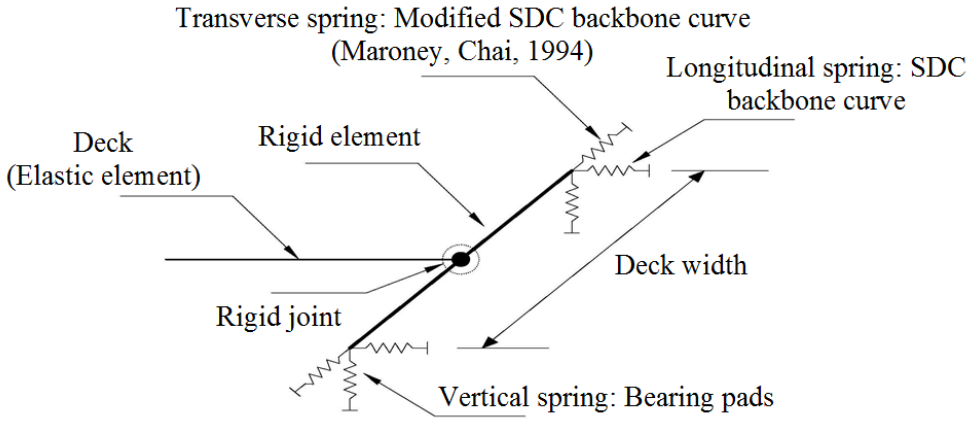

Fig. 3 Components of "simplified" mechanism for abutment modeling

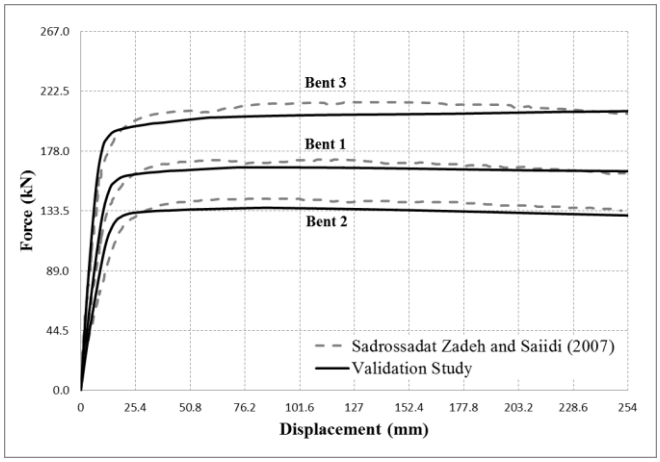

Fig. 4 Push-over capacity curves of bridge's bents in validation study

Table 3 Comparison of first six natural periods

Mode	Period (Sec.)	
	current study	Sadrossadat Zadeh and Saiidi (2007)
1	0.408	o.409
2	0.375	0.398
3	0.293	0.302
4	0.258	0.226
5	0.215	0.178
6	0.102	0.081

In order to validate the above mentioned modeling method, a numerical and shaking table experimental study at the University of Nevada was conducted on ¼ scaled bridge (Sadrossadat-Zadeh and Saiidi 2007). Both modal and push-over analyses were performed separately through the three-dimensional and two-dimensional (each bent) models, respectively. As it is shown in Fig. 4 and Table 3, acceptable accuracy in results of both analyses indicates a desired accuracy in numerical modeling. It is worth to note that abutment mechanism was not employed in this case and simple roller support at the abutments was considered for three dimensional modeling.

4. Input ground motions

Table 4 shows the used input ground motions which are selected from PEER (Pacific Earthquake Engineering Research Center) NGA database. The ground motions have been recorded on soil type II site (shear velocity of 375-750) and divided into far-fault and near-fault records. Since forward directivity pulse can be observed only in fault normal direction, the near-fault components of each station have been rotated to fault normal and parallel orientations. Moreover, the near-fault records have been adopted with a wide range of pulse periods so as to cover the first modes' vibration period of six different bridges. It is noted that the vertical component of

Table 4 Far-fault and near-fault sets of ground motions

Record No.	Name / Year	M	PGA	Pulse Period	Distance to Source	Scale Factor	
			g	Sec	km	DBE	MCE
Far fault ground motions							
1	Hector Mine / Hector -1999	7.1	0.34	----	----	3.433	5.153
2	Kobe / Nishi - Akashi-1995	6.9	0.51	----	----	3.252	4.881
3	Chi-Chi / CHY028-1999	7.6	0.79	----	----	1.676	2.516
4	Manjil / Abhar-1990	7.4	0.51	----	----	2.491	3.738
5	Chi-Chi / TCU045-1999	7.6	0.51	----	----	3.017	4.528
6	Friuli / Tolmezzo-1976	6.5	0.35	----	----	4.520	6.784
7	Chi-Chi /TCU095-1999	7.6	0.53	----	----	2.122	3.185
8	Northridge/Castaic -1994	6.69	0.49	----	----	2.245	3.369
9	Northridge / Mulhol-1994	6.69	0.51	----	----	3.335	5.006
10	Victoria / Cerro Prieto-1980	6.33	0.57	----	----	4.669	7.009
Near fault ground motions							
1	Coalinga-05 / Oil City-1983	5.8	0.87	0.7	4.1	----	4.163
2	Morgan Hill / Coyote Dam-1984	6.2	0.81	1	0.53	----	2.753
3	Chi-Chi/ CHY080-1999	6.2	0.47	1.4	22.37	----	2.439
4	Northridge-01 / LA Dam-1994	6.7	0.58	1.7	5.92	----	2.217
5	Chi-Chi / CHY006-1999	7.6	0.31	2.6	9.77	----	2.626
6	Cape Mendocino / Petrolia-1992	7	0.61	3	8.18	----	2.082
7	Northridge-01 / Jensen -1994	6.7	0.52	3.5	5.43	----	2.548
8	Chi-Chi / TCU076-1999	7.6	0.30	4	2.76	----	2.667
9	Bam / Bam-2003	6.5	0.80	4.3	1.0	----	1.411
10	Landers / Lucerne-1992	7.3	0.72	5.1	2.19	----	1.219

earthquake motions in near fault situation is under research and no unique observation has been reported about its importance on response parameters especially in strike-slip fault rupture. Moreover, considering both vertical and horizontal excitations in 3D directions complicates the analytical solutions and post processing of the results, however has not a meaningful effect on drift responses (Goel and Chopra 2009). Therefore, in the presented study the effect of vertical ground motion has been neglected.

In order to justify the results of nonlinear dynamic analysis in compare with recommendations of the common practice codes, input records in far-fault set should be scaled to actual seismic ground motion at appropriate level. The acceleration components scaled to site specific design spectrum of DBE level based on ASCE7 (2005) prevalent scaling procedure. The same procedure could not be applied to near-fault earthquakes, because the near-fault pulses would be attenuated unrealistically in this method. Subsequently, the ASCE7 (2010) proposed scaling method has been employed in this study. According to this procedure, each pair of components is rotated to the fault-normal and fault-parallel directions of the causative fault and then scaled; meanwhile, the average of the fault-normal components should not be less than the MCE response spectrum for

the period ranging from 0.2T to 1.5 T. Consequently, the presented procedure makes the average of scale factors in two record sets of far-fault and near-fault earthquake be close to each other, especially for ordinary structures with natural periods around 1.00 second. Additionally, to have better comparison between two types of ground motions and evaluating their effects on seismic behavior of bridges, far-fault records have been normalized to MCE level as well. In the scaling procedure, the 5% damping acceleration spectrum of the soil type II has been chosen based on Iranian earthquake code (2005).

Fig. 5 illustrates the response acceleration spectra of two sets of records. The graphs in this figure indicate that near-fault spectra have excessive variation with higher amplitudes in compare to far fault sets. So that it can cause a wide range of responses in structures and it could be the reason of some illustration in the result interpretation. Furthermore, Fig. 6 compares the averages of near-fault and far-fault spectra (SRSS component) before and after scaling for the case study bridge (model No.1). It can be inferred that there is a significant difference between near-fault and far-faults graphs within a common range of design periods (about 1.0-2.0 sec) and the difference could be obvious after scaling procedure. It could also be noticed that the average of acceleration spectrums of far-fault set which is scaled to MCE level has higher amplitude than that of others, however near-fault spectra approaches to MCE level of far-fault spectrum in the long period region. This can be explained by the role of near-fault ground motion records especially in long period systems. The scale factors of ground motions at different levels in the case study model

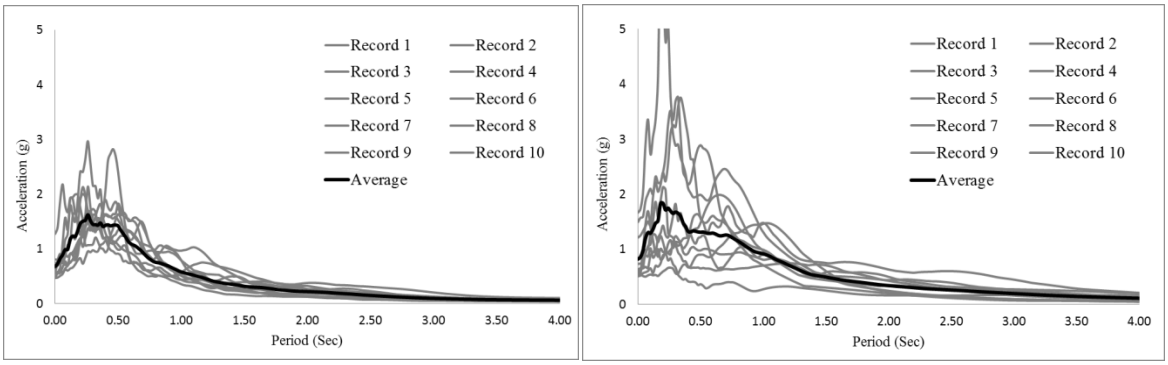

Fig. 5 SRSS normalized records of far-fault (Left) and near-fault (Right) sets

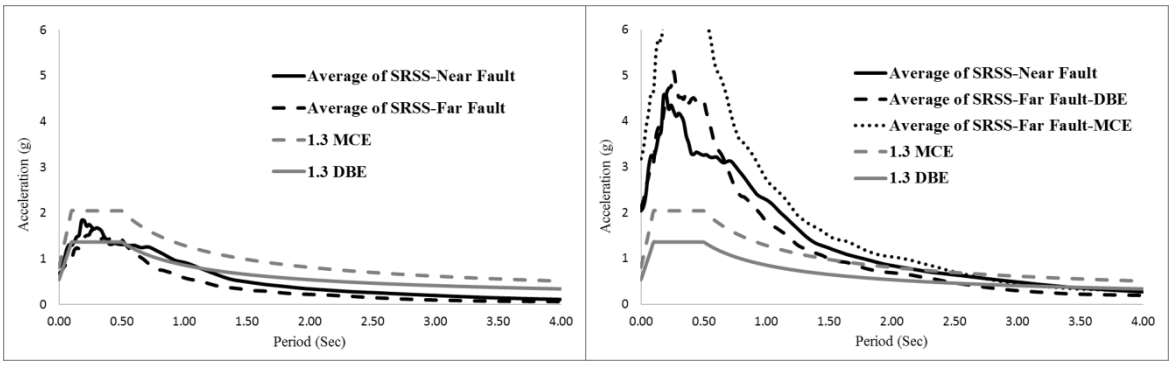

Fig. 6 Average of SRSS spectra of near-fault earthquakes before scaling (Left) and after scaling (Right) applicable to model 1

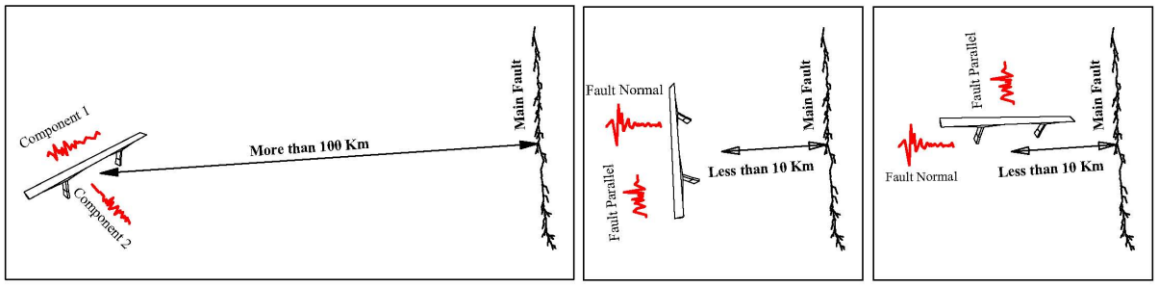

FF DBE/ FF MCE FN in T FN in L

Fig. 7 Schematic presentations for different scenarios

(model No. 1) are provided in Table 4. The averages of scale factors for far-fault earthquake, scaled into DBE and MCE levels, are 3.08 and 4.62 respectively and the value is about 2.41 for near-fault earthquakes. The comparison of the values shows that the scale factors for all near-fault records are less than those for far-fault ground motions at DBE and MCE levels in which it could be as an important parameter in comparing the following results.

5. Providing different scenarios for input motions

It is well established that forward directivity effects depend on source-to-site geometry. Several source-to-site geometric parameters have been used in the past to predict directivity effects of a site (Somerville *et al*. 1997). Although pulse velocity caused by directivity effects are expected to be found in the fault-normal component of the near-fault records many pulse-like ground motions are also observed in a range of orientations (Shahi and Baker 2011). Consequently, seismic performance of bridges under pulse-like ground motions was investigated in the extreme scenario which is fault normal component (pulse-liked component). This worst case scenario in highway bridges would be parallel to transverse or longitudinal directions of the viaduct. The chosen scenarios of the current research are illustrated in Fig. 7. Each scenario could be the controlling scenario depending on the characteristics of structure and input motions. Herein, these two extreme scenarios have been described as the fault normal component of near fault ground motions along the transverse direction of bridge (FN in T) and longitudinal direction of bridge (FN in L). Also far-fault ground motions scenarios at two levels of DBE and MCE have been named as "FF DBE" and "FF MCE", respectively.

6. Result of analysis

6.1 Drift ratio in piers

In order to have better understanding of the seismic behavior of the highway bridge, all proposed models were analyzed under near and far-fault records through 240 non-linear time history analyses. Table 5 provides the average values of maximum drift ratios in longitudinal and transverse directions of piers with their variances under far fault earthquakes in both DBE and

Table 5 Average of drift ratios at piers in longitudinal and transverse directions with their variances under far-fault record set

Models	Scenario	Longitudinal						Transverse					
		Pier 1	σ	Pier 2	σ	Pier 3	σ	Pier 1	σ	Pier 2	σ	Pier 3	σ
1	FF DBE	1.73	0.23	1.73	0.24	----	----	1.71	0.36	1.71	0.36	----	----
	FF MCE	2.19	0.32	2.19	0.32	----	----	2.67	1.66	2.67	1.65	----	----
2	FF DBE	1.61	0.26	1.61	0.26	----	----	2.05	1.05	1.31	0.17	----	----
	FF MCE	2.12	0.23	2.12	0.23	----	----	2.79	1.29	2.04	0.50	----	----
3	FF DBE	1.27	0.17	1.96	0.40	----	----	1.43	0.30	1.56	0.33	----	----
	FF MCE	1.77	0.20	2.75	0.48	----	----	2.13	0.53	3.01	1.19	----	----
4	FF DBE	1.86	0.34	1.86	0.34	1.86	0.34	1.96	0.49	2.35	0.61	1.97	0.51
	FF MCE	3.04	0.73	3.04	0.73	3.03	0.73	3.47	1.62	3.95	2.15	3.44	1.57
5	FF DBE	1.77	0.23	1.77	0.23	1.77	0.23	2.07	0.45	1.84	0.43	1.69	0.38
	FF MCE	2.33	0.31	2.33	0.31	2.33	0.31	3.07	1.26	3.03	1.36	2.88	1.16
6	FF DBE	1.52	0.24	1.94	0.38	2.53	0.66	1.75	0.33	2.07	0.67	2.17	0.70
	FF MCE	1.89	0.32	2.41	0.52	3.16	0.89	2.53	0.87	3.67	2.48	3.95	2.73

MCE scenarios. As it is expected, regular bridges (model 1 and 4) have uniform distribution of drifts ratios between the piers. Bridges with irregularity in span ratio (models 2 and 5) have uniform drift ratios due to same height of the piers in longitudinal direction. The maximum drift ratios are 1.61% and 1.77% at DBE level in models 2 and 5, respectively. The ratios are increased to 1.3 times at MCE level. In transverse direction the seismic performance of piers due to their individual behavior is more affected by the system irregularity so that the lower stiffened piers have larger drift ratio (maximum drift reaches to 2.0% and 3% at DBE and MCE levels, respectively). Furthermore, bridges with irregularity in height of piers (model 3 and 6) have the highest drift ratio at the shorter pier (stiffened pier) in both longitudinal and transverse directions. The maximum drift ratios in longitudinal direction approach to 1.96% and 2.53% at DBE level in models 3 and 6 respectively. The ratios in transverse direction are about 1.56% and 2.17%. Moreover, the values are increased to about 1.5 to 2.0 times at MCE level; however the transverse direction is more influenced by the strong ground motion (MCE level).

Furthermore, Table 6 provides the average values of maximum drift ratios in longitudinal and transverse directions of piers with their variances under directivity component of near-fault earthquakes in both FN in L and FN in T scenarios. The result indicates on the same distribution pattern of drift ratios under both near and far fault earthquakes at different regular and irregular models. However the irregular bridges have higher response than regular ones. Moreover, the maximum drift ratios of fault-normal components are higher than those of far-fault ones at both DBE and MCE levels, It is of paramount importance to point out the scaling factors in far-fault records (FF DBE and MCE) are higher than those of near-fault records. The average of maximum drift ratios under near-fault ground motions is about 1.5 to 2.2 times the same parameter at DBE level and about 1.0 to 1.3 at MCE level of far-fault earthquakes.

In irregular bridges, particularly those with irregularity in the height of piers, the ratio increases into the highest value. The other important point of the drift results is the significant dispersion among drift demands under near-fault responses. This shows the importance of results under

Table 6 Average of drift ratios at piers in longitudinal and transverse directions with their variances under far-fault record set

Models	Longitudinal						Transverse					
	Pier 1	σ	Pier 2	σ	Pier 3	σ	Pier 1	σ	Pier 2	σ	Pier 3	σ
	FNL Scenario						FNT Scenario					
Model 1	2.91	1.46	2.91	1.46	----	----	2.87	2.26	2.87	2.30	----	----
Model 2	2.65	1.32	2.65	1.32	----	----	3.47	3.04	2.78	1.58	----	----
Model 3	2.23	0.97	3.45	2.32	----	----	2.67	1.58	3.51	2.32	----	----
Model 4	3.63	2.00	3.63	2.00	3.63	2.00	3.47	2.76	3.99	3.29	3.44	2.71
Model 5	3.07	1.74	3.07	1.74	3.07	1.73	3.48	3.02	3.30	2.99	3.22	2.26
Model 6	2.54	1.26	3.24	2.05	4.25	3.51	2.85	1.74	3.79	2.18	3.99	2.97

almost all near-fault pulse-like ground motions, while the same order of drift distribution can be observed in all models. However, the presence of dispersion among earthquake responses depends on record selection and it is deemed acceptable by the engineers; the value of dispersion is so high that it could not be neglected. The primary reason could be found in the nature of near-fault earthquakes which are so sporadic, but a better reason could be expressed as the amplification phenomena under near-fault pulses due to narrow band effect. This phenomenon has previously been addressed by other researchers (Kalkan and Kunnath 2006, Champion and Leil 2012).

Based on limit states defined for material modeling, strength degradation and consequently collapse are modeled. The results show that, as an average, regular bridges in 2 out of 10 near-fault records and irregular bridges (Model 3 and 6) in 4 out of 10 near-fault records are in high risk of collapse. However under far-fault motions, there are no significant damages expected at DBE level. It can be concluded, seismic design procedure of AASHTO needs more restricted provisions for bridge in close distance of causative faults.

6.2 "Narrowband" effect in highway bridges

First researches on the near-fault pulses showed that the elastic structures with fundamental periods close to the near-fault pulse periods would be affected more (Somerville *et al*. 1997). This result exhibits the so-called "narrowband" effect. Further investigation revealed that the most damaging case for inelastic responses is found around the period ratio T/Tp=0.5 (Tp is the period of the primary pulse presented in the ground motion velocity time history and T is the elastic period of an oscillator). This is due to the significant elongation of natural period under inelastic behavior (Champion and Leil 2012). Therefore, it is desired to recognize the range of T/Tp for the developed models to have a better assessment of the effects of pulse-like ground motions on highway bridges. Herein, near-fault records have been selected in a way that their pulse periods (Tp) cover the range of fundamental period of the regular and irregular bridges. Fig. 8 shows the maximum drift of piers in different models under different pulse-like ground motions. In this figure, "narrowband" effect is observed in the T/Tp values between 0.3 and 0.5 in longitudinal, and between 0.5 and 0.6 in transverse directions. The T/Tp values obtained from the current research are lower than the other reported values. One of the primary reasons could be the contribution of abutment behavior in elastic and inelastic responses due to period lengthening and higher mode effects. The opening and closing of expansion gaps at the end of deck may change the first natural

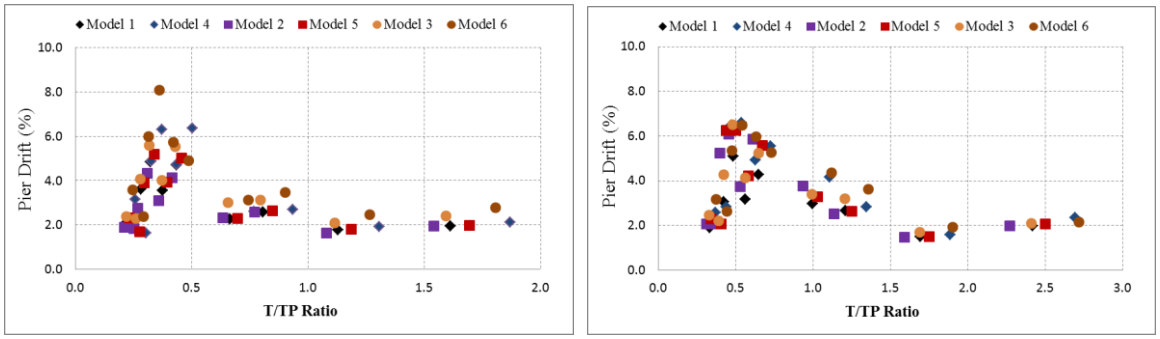

Fig. 8 Maximum pier drift versus bridge period to pulse period ratios in (a) longitudinal and (b) transverse directions

periods before full non-linearity is developed. This implies that the ratio of T/T_p which is affected by gap behavior is different from that of buildings.

6.3 Input and hysteretic energy trade off

Mean values of energy ratios (hysteretic energy/Input energy) for three models No.4, No.5 and No.6 in longitudinal and transverse direction of each pier and abutment are shown in Fig. 9. The figure shows the energy ratio varies between 12 to 23 percent in regular model No.4 (except the abutments in transverse direction) and also it is uniformly distributed among the piers and abutments. In bridges with irregularity in span (model No.5), the distribution of the ratios in both directions shares the same pattern as the regular model. Moreover, the ratio of pier 1 is smaller than the others due to the pier's tributary mass, which is about 47% of other piers. In the bridge with irregularity in height of piers, the energy ratio distribution is different from that in the other models. This figure shows that the shorter pier suffers greater damage so that more than 28 percent of total energy ratio is assigned to it. This non-uniform distribution is more obvious in longitudinal direction for both near- and far-fault records due to frame action of structure. Furthermore, the figure illustrates that distribution of energy ratio among the piers of different models is not changed significantly under near fault analyses. It indicates the participation of irregular parameters in both near-fault and far-fault records are the same (similar to drift ratio distribution). Moreover, in longitudinal direction of regular and irregular bridges, left abutments absorb more energy ratio in comparison with the right ones. This could be due to the effect of one directional high amplitude near-fault pulses in which the abutment does not respond symmetrically in longitudinal direction. As a result, a large residual displacement in the structure would be occurred (Phan *et al*. 2007).

In order to further investigate the problem, detailed input and hysteretic energies of different components are investigated in case study bridge. Fig. 10 shows time histories of energy, velocity, maximum drift and also hysteretic response of piers in longitudinal direction. Moreover, this figure provides total input energy (*Ei*), hysteretic energy of Piers (WH-Pier), hysteretic energy of abutments (WH-Abut) and kinetic energy (WK) under record No.6 (near fault) and record No.10 (far fault) at DBE and MCE levels. A sample of plastic hinge's hysteresis response is illustrated in this figure as well. The presented result shows that the maxima of drift and velocity time histories

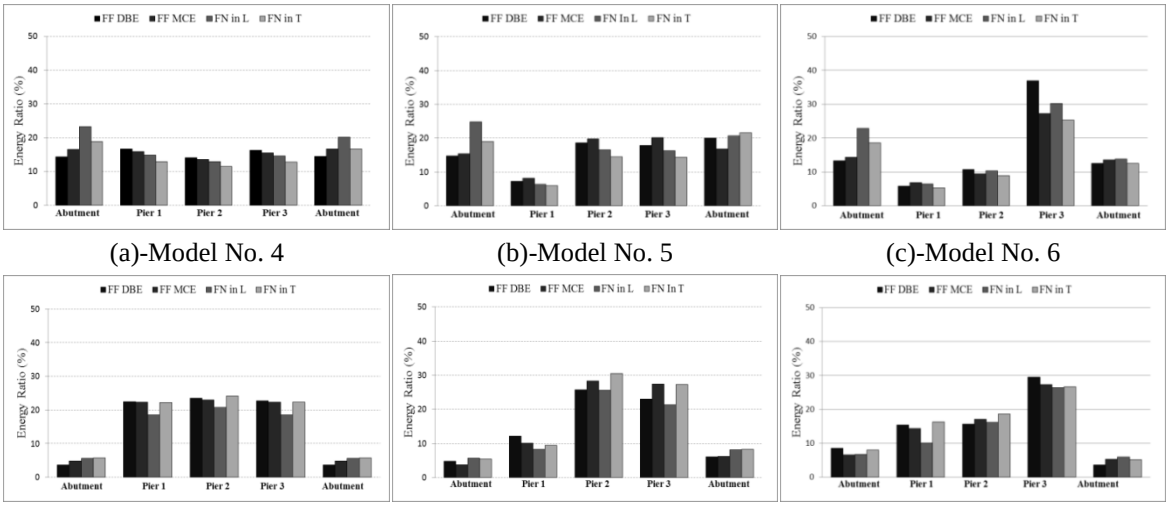

(a)-Model No. 4 (b)-Model No. 5 (c)-Model No. 6

(d)-Model No. 4 (e)-Model No. 5 (e)-Model No. 5

Fig. 9 Energy ratio for Model No. 4, No. 5 and No. 6 in Longitudinal direction (a, b and c) and Transverse direction (d, e and f)

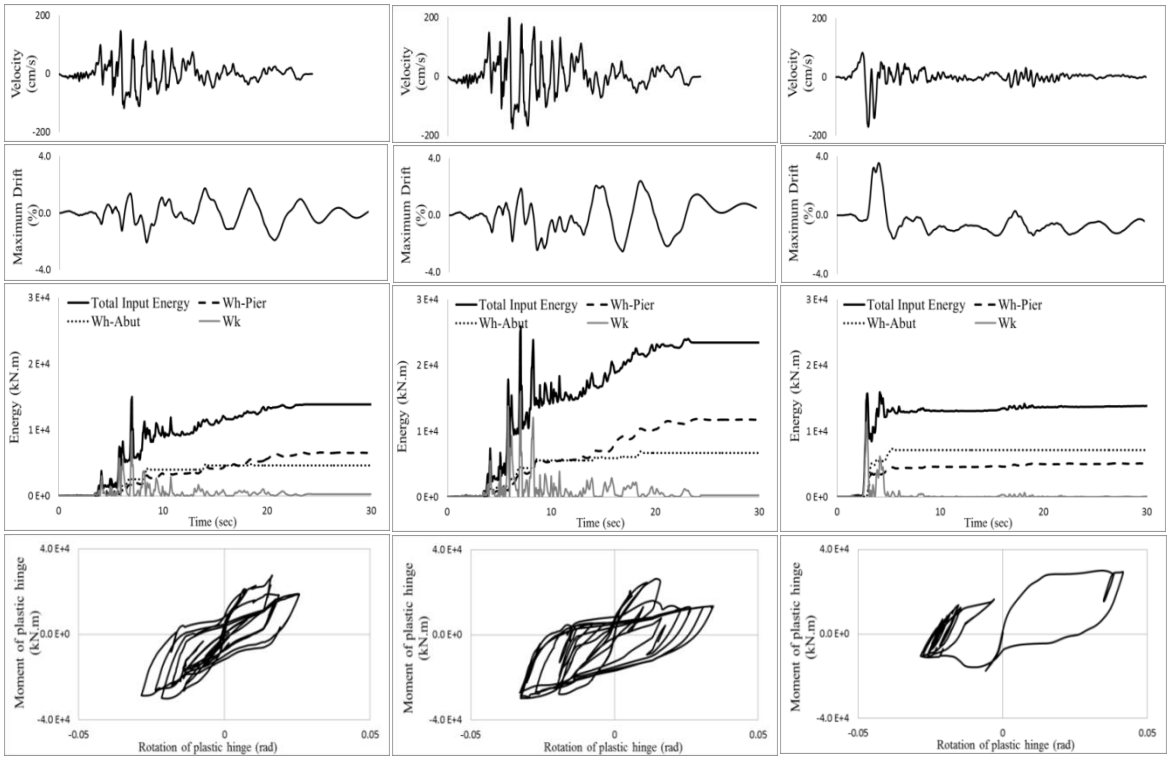

(a) (b) (c)

Fig. 10 Velocity record No 6. ((a) FF DBE, (b) FF MCE) and No.10 ((c) FN in T) and their corresponding energy time history and hysteretic diagram of pier in model No. 1 in longitudinal direction

of fault normal component reach the peak at the same time. The peak value of velocity time history in this component is about 1.16 and 0.77 times the far-fault ground motion at DBE and MCE levels, respectively. Furthermore, energy time history of pulse-like ground motion, input energy and consequently hysteretic energy reach maximum values in a very short time (in this case it is about ¼ the times of the far-fault one) and it causes piers to dissipate a large amount of energy in a short time. Consequently, this phenomenon results into higher ductility demand in piers and it should be considered in structural design of high way bridges. In this figure hysteretic response of pier under pulse-like motion has fewer hysteresis loops with higher rotation amplitude in comparison with the far-fault results. This configuration has lower amount of dissipated energy (32% of total input energy) with respect to the same parameter under far-fault record (45% of total input energy). This is an important subject that is reported by other researchers in other structures (Kalkan and Kunnath 2006).

Figs. 9 and 10 show larger fraction of energy has been dissipated by the abutment under near-fault motions due to higher displacement demand of piers. The ratio of dissipated energy in abutment to total input energy under near field motion is about 0.46 and under far-fault is reduced to 0.30. These results indicate that hysteretic energy and ductility demands under near-fault pulse like ground motions are completely different than same parameters when bridges are under far-fault motions and it should be considered in modern design procedures.

6.4 Damage indexes in different scenarios

The evidence by many researches is growing that drift ratio individually is not a proper measure for evaluating damage when a structure is subjected to low amplitude and long duration ground motion. As it was described in previous section, the amount of dissipated energy during an earthquake is a key parameter for indicating damage in structures. Therefore the combination of two parameters, drift and dissipated energy ratios, introduces an index to properly evaluate the total damage of structure. In current study, a well-known damage index (DI) which has been introduced by Park *et al*. (1985) is employed to evaluate structural damages of piers in different models. The most important parameter in DI is the coefficient of hysteretic energy ratio which is denoted as β. Cosenza *et al*. (1993) proposed the median value of 0.15 for this parameter based on a set of ordinary long-duration far-fault records. Herein, DI is used so as to clarify how both dissipated energy and drift ratio of pier can be affected under near-fault pulses.

The result of damage index ratios for all samples is shown in Fig. 11.The derived DI values for irregular bridges show that irregularity in span does not change the bridge's damage pattern significantly. Whereas, the bridges with irregularity in height of pier show more than 20% increase in DI values in comparison with the regular ones. It is also shown that influence of near fault ground motions does not change DI distribution pattern; however significant increase can be observed in DI values under near-fault earthquakes. It should be considered that DI values under near fault motions are close to MCE levels of far fault earthquakes while its scale factor is considerably lower. The amount of DIs under near-fault pulses are about 1.6 and 1.0 times of the far-fault records in DBE and MCE levels, respectively.

Furthermore, Table 7 shows the contribution ratio of relative displacement of pier to hysteretic energy in damage index for all bridge cases under different earthquakes. According to the table, this ratio under near fault motions is about 1.2~1.5 times greater that under far fault ones (DBE and MCE levels). The ratio also increases with increasing degree of irregularity in structure due to higher level of damage concentration in irregular bridges under pulse-like motions.

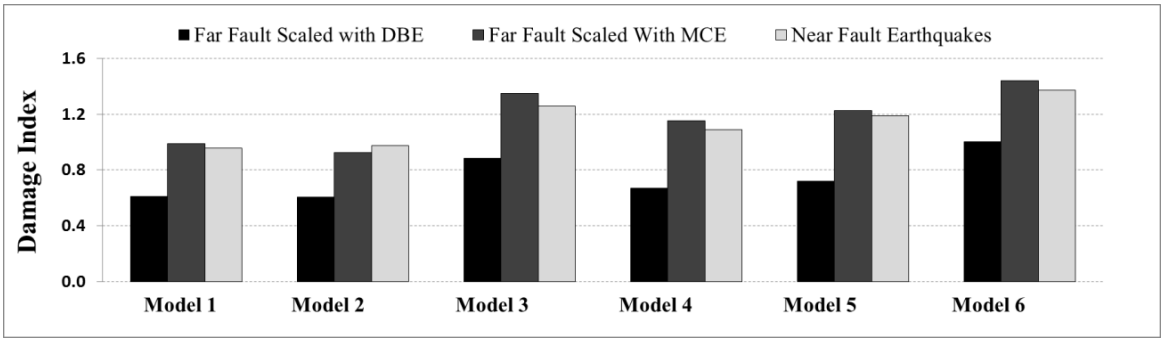

Fig. 11 the mean of damage index (DI) of different models under different earthquakes

Table 7 The contribution ratio of relative displacement of pier to hysteretic energy in damage index

Earthquake	Model 1	Model 2	Model 3	Model 4	Model 5	Model 6
Far Fault Scaled with DBE	1.44	1.66	1.38	1.49	1.63	1.81
Far Fault Scaled with DBE	1.71	1.66	1.88	1.71	1.95	2.71
Near Fault Earthquakes	2.51	2.84	3.20	3.03	3.17	3.72

This could be illustrated using the nature of the hysteretic loops of plastic hinges under near fault earthquakes (see Fig. 10). According to this configuration more displacement ductility is required with lower amount of hysteretic energy and it can be concluded that under near fault motions, the contribution ratio of relative displacement of pier to hysteretic energy in damage index is significantly increased. The value of 0.15 for β is consistent with ordinary far fault records; however it should be adjusted for stronger near fault motions. It seems, the shorter rising time (time in which input energy reaches to more than 95% of its value) in near fault pulse like motions changes the participation of different components of DI and affects the value of β.

7. Conclusions

In this study, seismic performance of regular and irregular framed box girder Highway Bridges under an ensemble of near-and far-fault ground motions has been investigated. Through the four different scenarios (FF DBE, FF MCE, NF in L and NF in T), near-fault ground motions have been compared with the far-fault ones at DBE and MCE levels. The scenarios have been chosen based on fault rupture direction in regarding with bridge position so as to study forward directivity pulses in each direction of piers. The seismic demand parameters such as drift ratio, hysteretic energy, input energy, and damage index (DI) of the pier in different scenarios are computed in longitudinal and transverse directions of regular and irregular models. The major obtained results are summarized as follows:

• Regular and irregular bridges have almost the same distribution pattern of drift ratios under both near and far-fault records, however the irregular bridges are influenced more by near fault pulses.

• The maximum response of bridges with irregularity in height is taking place in the shorter pier in both directions. Nonetheless, the bridges with irregularity in span ratios have the higher

response in piers near the shorter span in transverse direction.

• Collapse of the bridges under near-fault pulse like ground motions is more probable than far-fault motions. Under near-fault pulses, seismic drift of piers is about 2.0 times the far-fault records at DBE level and 1.3 times the same records at MCE level.

• The hysteretic energy under near-fault earthquakes is lower than that of far-fault ground motions. This can be explained by the hysteretic loops configuration which contains fewer numbers of loops and has loops with extreme value of rotation under near-fault ground motion.

• Due to the large deformation of a structure under near-fault earthquake, the abutments dissipate more energy which reduces the structural demand in piers.

• "Narrowband" effect is observed in a ratio (T/Tp) between 0.3 and 0.5 in longitudinal direction and between 0.5 and 0.6 in transverse direction. (T is the period of first mode of structure, Tp is pulse period).

• The contribution ratio of relative displacement of pier to hysteretic energy in damage index under near-fault pulse like motions is higher than for far fault motion. In order to have more accurate criteria, the hysteretic coefficient in damage index formulation (β) should be adjusted for near fault earthquakes to have realistic damage criteria.

References

AASHTO (2007), *Standard Specifications for Highway Bridges*, American Association of State Highway and Transportation Officials, Washington, D.C.

Alavi, B. and Krawinkler, H. (2001), "Effects of near-fault ground motions on frame structures", Ph.D. Dissertation, Stanford University, CA.

ASCE/SEI 7 (2005), *Minimum Design Loads for Buildings and Other Structures*, American Society of Civil Engineers, USA.

ASCE/SEI 7 (2010), *Minimum Design Loads for Buildings and Other Structures,* American Society of Civil Engineers, USA.

Aviram, A., Mackie, K.R. and Stojadinović, B. (2008), "Guidelines for Nonlinear Analysis of Bridge Structures in California", *Pacific Earthquake Engineering Center (PEER)*.

Bonvalot, E. (2006), "Dynamic response of bridges to near-fault forward directivity ground motions", M.Sc. Dissertation, Washington State University, Washington.

Caltrans (2006), *Seismic Design Criteria (SDC)*, California Department of Transportation, Sacramento, California.

Champion, C. and Leil, A. (2012), "The effect of near-fault directivity on building seismic collapse risk earthquake", *Eng. Struct. Dyn.*, **41**(10), 1391-1409.

Cosenza, E., Manfredi, G. and Ramasco, R. (1993), "The use of damage functionals in earthquake engineering: A comparison between different methods", *Earthq. Eng. Struct. Dyn.*, **22**, 855-868.

Goel, R.K. and Chopra, A.K. (2009), "Nonlinear analysis of ordinary bridges crossing fault rupture zones", *J. Bridge Eng*., ASCE, **14**(3), 216-244.

Iranian Code of Practice for Seismic Resistant Design of Buildings-Standard (2005), 2800- 05, 3rd Edition.

Kalkan, E. and Kunnath, S.K. (2006), "Effects of fling step and forward directivity on seismic response of buildings", *Earthq. Spec*., **22**(2), 367-390.

Liao, W.I., Loh, C.H., Wan, S., Jean, W.Y. and Chai, J.F. (2000), "Dynamic responses of bridges subjected to near-fault ground motions", *J. Chinese Inst. Eng.*, **23**(4), 455-64.

Mander, J.B., Priestley, M.J.N. and Park, R. (1998), "Theoretical stress-strain model for confined concrete", *J. Struct. Eng.*, ASCE, **114**(8), 1804-1849.

Maroney, B.H. and Chai, Y.H. (1994), "Seismic design and retrofitting of reinforced concrete bridges", *Proceedings of the 2nd International Workshop on Earthquake Engineering (Earthquake Commission of*

New Zealand, Queenstown), New Zealand.
Mayes, R.L. and Shaw, A. (1997), "The effects of near fault ground motions on bridge columns", *Proceeding of the FHWA/NCEER Workshop on the National Representation of Seismic Ground Motion for New and Existing Highway Facilities*, Burlingame, California.
Mckenna, F., Fenves, G.L., Scott, M.H. and Jeremić, B. (2010), "Open system for earthquake engineering simulation", University of California, Berkeley, CA.
Orozco, G.L. and Ashford, S.A. (2002), "Effects of large velocity pulses on reinforced concrete bridge columns", Pacific Earthquake Engineering Research Center (PEER), University of California, Berkeley, CA.
Park, Y.J., Ang, A.H.S. and Wen, Y.K. (1985), "Seismic damage analysis of reinforced concrete buildings", *J. Struct. Eng.*, ASCE, **4**(740), 111.
Park, S.W., Ghasemi, H., Shen, J., Somerville, P.G., Yen, W.P. and Yasinsky, M. (2004), "Simulation of the seismic performance of the Bolu viaduct subject to near-fault ground motions", *Earthq. Eng. Struct. Dyn.*, **33**, 1249-1270.
PEER Strong Motion Catalog, http://peer.berkeley.edu/smcat
Phan, V., Saiidi, S., Anderson, J. and Ghasemi, H. (2007), "Near fault ground motion effect on reinforced concrete bridge columns", *J. Struct. Eng.*, ASCE, **133**(7), 982-989.
Sadrossadat-Zadeh, M. and Saiidi, S. (2007), "Pre-test analytical studies of NEESR-SG 4-Span bridge model using open sees", Center of Civil Eng. Earthq. Res., University of Nevada, Reno, USA.
Shahi, S. and Baker, J. (2011), "An empirically calibrated framework for including the effects of near-fault directivity in probabilistic seismic hazard analysis", *Bul. Seismol. Soc. Am.*, **101**(2), 742-755.
Somerville, P.G., Smith, N.F., Graves, R.W. and Abrahamson, N.A. (1997), "Modification of empirical strong ground motion attenuation relations to include the amplitude and duration effects of rupture directivity", *Seismol. Res. Lett.*, **68**(1), 199-222.
Wilson, P. and Elgamal, A. (2006), "Large scale measurement of lateral earth pressure on bridge abutment back-wall subjected to static and dynamic loading", *Proceedings of the New Zealand Workshop on Geotechnical Earthquake Engineering*, University of Canterbury, Christchurch, New Zealand.

SA